# Minimization of proteome reallocation explains metabolic transition in hierarchical utilization of carbon sources

Zhihao Liu[1,2], Minghao Chen[1], Jingmin Hu[1], Yonghong Wang[1*], Yu Chen[2*]

1 State Key Laboratory of Bioreactor Engineering, East China University of Science and Technology, Shanghai 200237, China

2 Key Laboratory of Quantitative Synthetic Biology, Shenzhen Institute of Synthetic Biology, Shenzhen Institute of Advanced Technology, Chinese Academy of Sciences, Shenzhen 518055, China

* Corresponding authors:

Yonghong Wang (yhwang@ecust.edu.cn)

Yu Chen (y.chen3@siat.ac.cn)

**Keywords:** enzyme constraint, metabolic model, mixed carbon sources, metabolic transition

**Abstract**

Cells choose between alternative pathways in metabolic networks under diverse environmental conditions, but the principles governing the choice are insufficiently understood, especially in response to dynamically changing conditions. Here we observed that a lactic acid bacterium *Bacillus coagulans* displayed homolactic fermentation on glucose or trehalose as the sole carbon source, but transitioned from homolactic to heterolactic fermentation during the hierarchical utilization of glucose and trehalose when growing on the mixture. We simulated the observation by dynamic minimization of reallocation of proteome (dMORP) using an enzyme-constrained genome-scale metabolic model of *B. coagulans*, which coincided with our omics data. Moreover, we evolved strains to co-utilize mixed carbon sources, circumventing the hierarchical utilization and inactivating the choice of heterolactic fermentation. Altogether, the findings suggest that upon rapid environmental changes bacteria tend to minimize proteome reallocation and accordingly adjust metabolism, and dMORP would be useful in simulating and understanding cellular dynamics.

## Introduction

Cells have alternative pathways, i.e., redundancy, in metabolic networks to adapt to diverse environmental conditions. For instance, while many microbes and mammalian cells use respiration for ATP production, some of them also harbor fermentation as an alternative ATP-producing pathway, which enables not only survival under anaerobic conditions but also fast growth in the presence of oxygen, i.e., aerobic fermentation[1]. The alternative pathways empower cells to choose between distinct metabolic strategies, but the principles governing the cellular choice are insufficiently understood[2].

Experimental and theoretical studies suggest that the choices of alternative pathways and metabolic strategies reflect tradeoffs, mostly between metabolic efficiency, e.g., yield, of pathways and cellular resources, e.g., proteome, invested for enzymes of the pathways[3-8]. For instance, fermentation has a lower ATP yield but is more proteome efficient than respiration, and therefore favors fast-growing cells subject to the limited proteome resources[9,10]. These studies are predominantly focused on steady-state cultures, e.g., chemostats, of model microbes, and therefore the cellular choice might be a result of a relatively long-term adaption to the environment. However, much less is known whether and how cells can transition between alternative pathways under dynamically changing environments, which are ubiquitous in both natural and artificial biological systems[11,12].

Here we studied a lactic acid bacterium *Bacillus coagulans*, which has alternative pathways converting glycolytic carbon sources to lactate, i.e., homolactic and heterolactic fermentation[13,14]. The former converts carbon sources to lactate via the Embden–Meyerhof–Parnas (EMP) pathway, while the later the phosphoketolase pathway with a lower lactate yield[15,16]. We observed that *B. coagulans* displayed the homolactic fermentation on glucose or trehalose as the sole carbon source, but transitioned from homolactic to heterolactic fermentation in the hierarchical utilization of glucose and trehalose when growing on the mixture. We hypothesized that the metabolic transition could be interpreted by dynamic minimization of reallocation of proteome, and performed enzyme-constrained metabolic modeling and omics analysis to test the hypothesis. Finally, by adaptive laboratory evolution (ALE) we evolved strains that can co-utilize the mixed carbon sources, inactivating the heterolactic fermentation.

## Results

### Lactate yield significantly changed in hierarchical utilization of glucose and trehalose

*B. coagulans* is widely used in the industrial lactate fermentation[14,17,18], where hydrolysates of low-cost starch-based materials are commonly used as the carbon sources[19,20] considering cost and benefit. However, the co-existence of multiple carbon sources in the medium may lead to the hierarchical utilization[21-26] and thus the waste of substrates[27], the extension of fermentation cycle [28] and the difficulty in product separation and purification[29]. Therefore, identifying the principles governing the dynamic behavior of *B. coagulans* during the hierarchical utilization of mixed carbon sources would be of significance from both basic and applied science perspectives.

We performed batch fermentation of *B. coagulans* on the mixture of glucose and trehalose, a disaccharide with a high percentage in the hydrolysates[30]. We observed the hierarchical

utilization of glucose and trehalose, which divided the entire fermentation process into three phases (Fig. 1A). In the glucose utilization phase ($P_{gluc}$, 0-12 h), glucose was exclusively consumed and lactate was rapidly produced with the lactate yield on glucose being 0.897 g/g, which was similar to the yield (i.e., 0.882 g/g) on glucose as the sole carbon source (Fig. 1B) and close to the yield of homolactic fermentation[15,31]. Upon glucose depletion, the lag phase occurred ($P_{lag}$, 12-16 h), in which the lactate production stopped, the biomass concentration (measured by $OD_{620}$) declined (Fig. 1A) and a few organic acids were slightly consumed (Supplementary Fig. 1). The growth arrest might be caused by other factors than depletion of nutrients, e.g., amino acids (Supplementary Fig. 2). In the trehalose utilization phase ($P_{tre}$, 16-84 h), trehalose was consumed, and lactate was produced again (Fig. 1A). Interestingly, the lactate yield on trehalose in $P_{tre}$ was only 0.526 g/g, which was much lower than that (i.e., 0.851 g/g) on trehalose as the sole substrate (Fig. 1B) and close to the theoretical lactate yield of heterolactic fermentation[15]. This was in line with the increased yields of byproducts in $P_{tre}$ (Supplementary Table 1). The significant change in the lactate yield during the hierarchical utilization of glucose and trehalose indicated distinct strategies to catabolize the carbon sources in $P_{gluc}$ and $P_{tre}$.

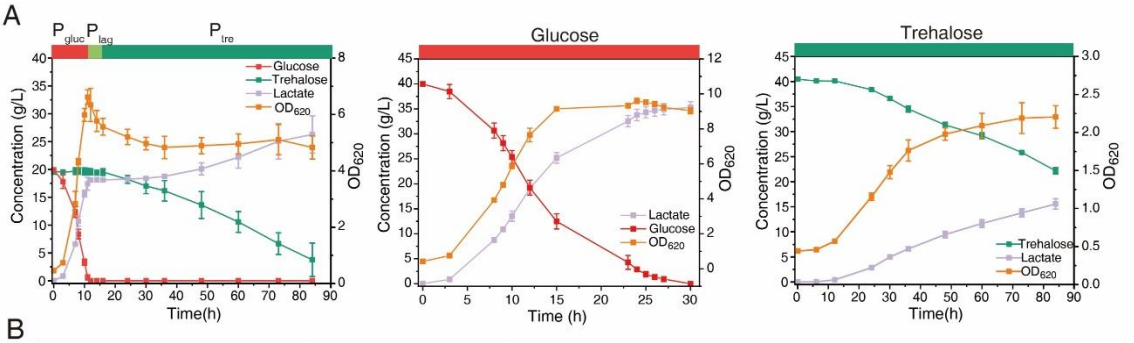


| Carbon source conditions | $P_{gluc}$ | $P_{tre}$ | Glucose | Trehalose |
|---|---|---|---|---|
| Lactate yield (g/g) | 0.897±0.015 | 0.526±0.041 | 0.882±0.006 | 0.851±0.044 |

**Figure 1. Fermentation on various carbon sources in 5 L bioreactor by *B. coagulans*.** (A) Fermentation processes on glucose and trehalose as the mixed carbon sources (left), sole glucose (middle) and sole trehalose (right). Data in the plots are shown with mean ± s.d. of three biological replicates. (B) Lactate yields under various phases and conditions. Data in the table are shown with mean ± s.d. of three biological replicates.

**Dynamic minimization of reallocation of proteome predicted metabolic changes**

To gain a systematic understanding, we reconstructed a genome-scale metabolic model of the strain *B. coagulans* DSM 1 = ATCC 7050[32] called iBcoa620, which was evaluated by the Memote score[33] and validated by growth on various carbon sources (Supplementary Fig. 3). Subsequently, we converted iBcoa620 into an enzyme-constrained version eciBcoa620 using the GECKO toolbox[34], allowing for understanding of metabolic changes by taking into account the enzyme usage and proteome allocation[35-37].

To predict the changes during the fermentation process, we performed dynamic flux balance analysis (dFBA)[38] with eciBcoa620 (Fig. 2A). The dFBA approach can divide the entire period into

multiple time intervals and obtain the flux distribution at each time interval by performing classical FBA[39] which requires a predefined objective function. While growth maximization as the objective function appeared reasonable to simulate for $P_{gluc}$, it could not predict the cellular behavior after glucose depletion (Fig. 2B), meaning that cells might adjust the objective in response to the changing environment. Therefore, we attempted other commonly used objective functions[40], including to maximize lactate production and to maximize non-growth-associated maintenance (NGAM), and found that they also failed to capture the cellular behavior in $P_{tre}$ (Supplementary Fig. 4), i.e., predicted either much higher lactate concentrations than measurements or no lactate production (Fig. 2B).

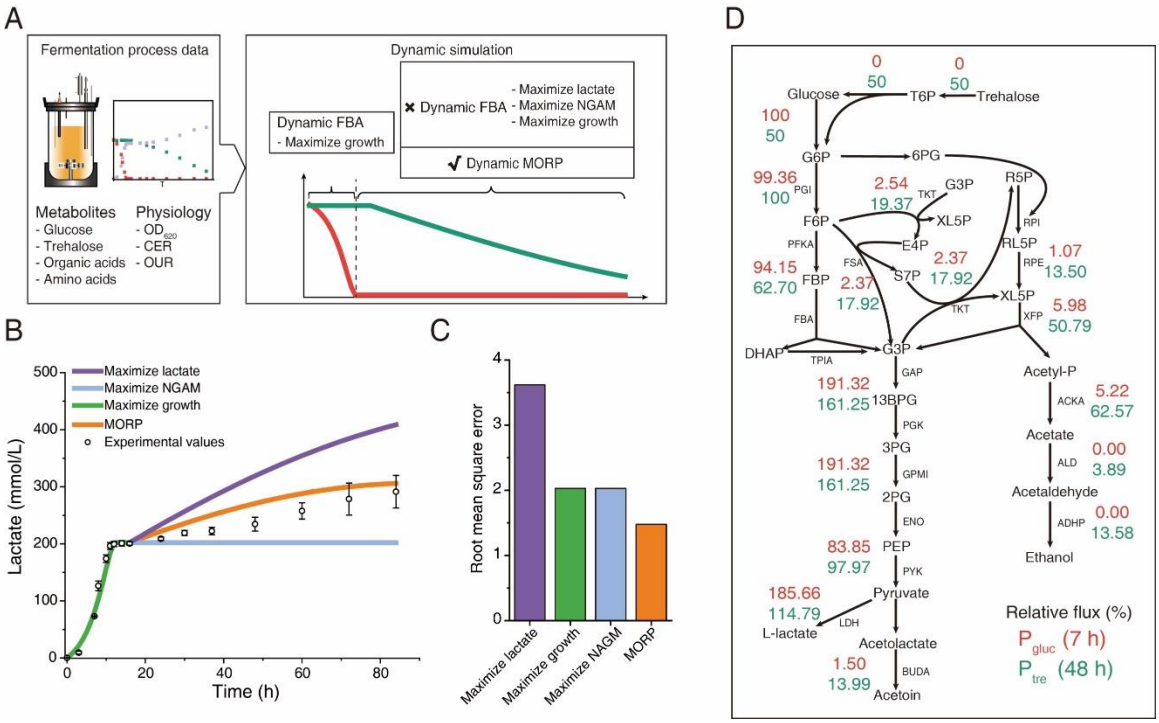


**Figure 2. Simulation of batch fermentation under mixed carbon sources by eciBcoa620.** (A) Simulation of the fermentation process. In the dFBA simulation of $P_{gluc}$ the growth rate was maximized. To simulate $P_{tre}$, various objective functions could be adopted within the dFBA framework. Additionally, we developed an approach to dynamically minimize the proteome reallocation with the enzyme-constrained models. (B) Simulation of lactate production using different objective functions. Minimization of proteome reallocation predicted the lactate production in $P_{tre}$ better than the others. Data in the plot are shown with mean ± s.d. of three biological replicates. (C) Root mean square errors of the different objective functions in predicting $P_{tre}$. Root mean square error quantifies the difference between the predicted and experimental concentrations of detected products, including lactate, acetate, pyruvate, acetoin and ethanol. (D) Comparison of the relative fluxes of the central carbon metabolism (CCM) between $P_{gluc}$ (represented by 7 h) and $P_{tre}$ (represented by 48h). Relative flux is calculated as the percentage of the absolute flux of each reaction to the substrate uptake flux. Note that one unit of trehalose uptake flux was converted to two units of glucose uptake flux. Abbreviations: T6P, trehalose 6‐phosphate; G6P, glucose 6‐phosphate; F6P, fructose 6‐phosphate; FBP, fructose 1,6‐

bisphosphate; DHAP, dihydroxyacetone phosphate; G3P, glyceraldehyde 3 - phosphate; 13BPG, glycerate 1,3 - bisphosphate; 3PG, 3-phosphoglycerate; 2PG, 2-Phospho-D-glycerate; PEP, phosphoenolpyruvate; 6PG, gluconate 6 - phosphate; E4P, erythrose 4 - phosphate; S7P, sedoheptulose 7-phosphate; R5P, ribose 5 - phosphate; RL5P, ribulose 5 - phosphate; XL5P, xylulose 5-phosphate; Acetyl-P, Acetyl phosphate; PGI, glucose-6-phosphate isomerase; PKFA, 6-phosphofructokinase; FBA, fructose-1,6-bisphosphate aldolase; GAP, glyceraldehyde-3-phosphate dehydrogenase; PGK, phosphoglycerate kinase; GPMI, phosphoglycerate mutase; ENO, enolase; PYK, pyruvate kinase; LDH, L-lactate dehydrogenase; RPI, ribose 5-phosphate isomerase; RPE, ribulose-phosphate 3-epimerase; XFP, phosphoketolase; FSA, fructose-6-phosphate aldolase; TKT, transketolase; BUDA, acetolactate decarboxylase; ACKA, acetate kinase; ALD, aldehyde dehydrogenase; ADHP, alcohol dehydrogenase.

Considering the fact that proteome reallocation requires frequent protein synthesis and degradation, which is of high cost to cells[40], we hypothesized that cells tend to dynamically minimize the proteome reallocation in response to rapid environmental changes. To test it, we developed the approach of minimization of reallocation of proteome (MORP) and extended to the dynamic version dMORP to simulate the cellular behavior after glucose depletion (Fig. 2A). The dMORP approach leverages the enzyme-constrained models and minimizes the sum of absolute differences of all enzyme usage values between previous and current time intervals (Materials and Methods). By employing dMORP, we found that the lactate production in $P_{tre}$ was well predicted (Fig. 2B). Moreover, dMORP outperformed other tested objective functions as it led to the smallest Root Mean Square Error (RMSE) (Fig. 2C) and it predicted production of byproducts in $P_{tre}$ such as acetate, acetoin and ethanol (Supplementary Fig. 4). Furthermore, we compared the metabolic fluxes predicted by various objective functions with those by random sampling, which enables unbiased estimations of metabolic fluxes subject to experimentally measured constraints. For reactions in the central carbon metabolism (CCM), the fluxes predicted by dMORP were generally within the ranges of the sampled fluxes, while the fluxes by other objective functions notably deviated (Supplementary Fig. 5). Therefore, we demonstrated that dMORP could be a more realistic objective function for describing the cellular behavior after glucose depletion.

To explain the observed lower lactate yield in $P_{tre}$ with dMORP, we compared the relative fluxes, i.e., normalized to carbon source uptake, of the CCM reactions in $P_{tre}$ (simulated at 48 h, i.e., middle in $P_{tre}$) to those in $P_{gluc}$ (simulated at 7 h, i.e., mid-exponential phase in $P_{gluc}$). We found in $P_{tre}$ a much greater fraction of carbon flux toward phosphoketolase (Fig. 2D), resulting in carbon loss in the form of acetate and ethanol and thereby the decreased lactate yield[14]. This was also similar with the comparison between $P_{tre}$ and the sole trehalose condition (Supplementary Fig. 6). In addition, we compared the absolute fluxes simulated at 7 h, 14 h and 48 h, representing $P_{gluc}$, $P_{lag}$ and $P_{tre}$, respectively (Fig. 3). We found that the metabolic fluxes in $P_{lag}$ and $P_{tre}$ were comparable and generally less than those in $P_{gluc}$ (Fig. 3), exemplified by the glycolytic fluxes, which was due to the considerably slower substrate uptake (Supplementary Table 1). By comparing $P_{gluc}$ and $P_{tre}$, we found that the reactions phosphoketolase, ribulose-phosphate 3-epimerase and acetate kinase displayed smaller changes in fluxes than glycolytic reactions

(Supplementary Fig. 7), which ensured an enhanced flux fraction in response to a large reduction in the substrate uptake flux, indicating their essential contribution to heterolactic fermentation, i.e., the low lactate yield.

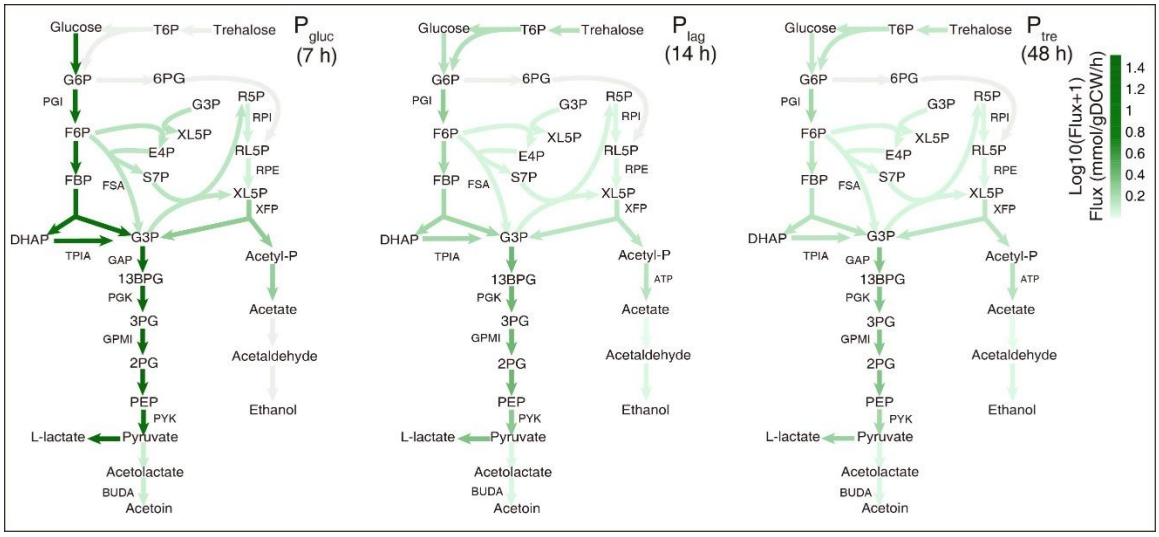


**Figure 3. Fluxes of the CCM reactions in the fermentation process predicted by eciBcoa620.** The metabolic flux distributions of the CCM at 7 h, 14 h, and 48 h. These three time points represent $P_{gluc}$, $P_{lag}$ and $P_{tre}$, respectively. At 7 h the objective function was to maximize growth while at 14 h and 48 h it was to minimize the proteome reallocation.

**Omics data coincided with dynamic minimization of proteome reallocation**

The enzyme-constrained model allowed us to investigate the enzyme usage based on the equation $v = k_{cat} \cdot e$, in which $v$ is the reaction rate (flux), $k_{cat}$ enzyme turnover number and $e$ enzyme usage. While the equality resulted in the same fold change in the flux and enzyme usage for most reactions between time intervals, some reactions, e.g., enriched in the glycolysis pathway, showed differences between fold changes in fluxes and enzyme usage when MORP was used as the objective function (Supplementary Fig. 8). By plotting the fold changes in fluxes and enzyme usage versus fermentation time for six glycolytic reactions, we found the divergence of the changes in fluxes and enzyme usage in $P_{lag}$ and $P_{tre}$ (Fig. 4), indicating the effectiveness of MORP.

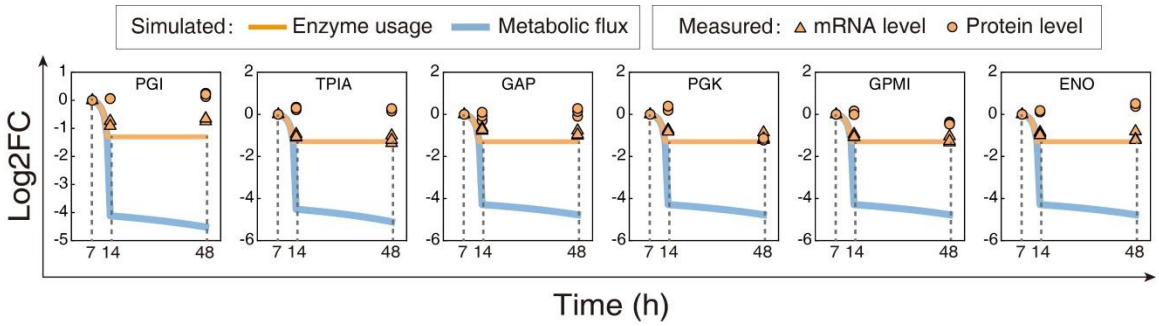

**Figure 4. Comparison between the simulations by dMORP and the omics data for glycolytic reactions.** The log2FC value represents the change in enzyme usage, metabolic flux, mRNA or protein level relative to the 7 h point. The enzyme usage and metabolic fluxes were predicted by dMORP, and the mRNA and protein levels were from measured transcriptomics and proteomics data with biological triplicates.

To systematically unravel the molecular mechanisms, we collected transcriptomics and proteomics data at 7 h, 14 h and 48 h, representing $P_{gluc}$, $P_{lag}$ and $P_{tre}$, respectively. The transcriptomics and proteomics data, which showed high consistency among biological triplicates while clear variability among different phases (Supplementary Fig. 9), were used for identifying differentially expressed transcripts and proteins (Materials and Methods). Enrichment analysis of the differential expression showed that from $P_{gluc}$ to $P_{lag}$ and $P_{tre}$ pathways were mostly downregulated, particularly those related to translation, e.g., ribosome and aminoacyl-tRNA biosynthesis (Supplementary Fig. 10), in line with the observed growth arrest (Fig. 1A). Moreover, the differential expression was enriched in amino acid pathways, which could be associated with the significant changes in the concentrations of intracellular amino acids (Supplementary Fig. 11).

The transcriptomics and proteomics data did not identify significant changes in the glycolysis pathway (Supplementary Fig. 10), coinciding with the simulated subtle changes in the usage of glycolytic enzymes. Notably, when plotting the measured changes in the mRNA and protein levels for the six glycolytic reactions, we observed similar trends with the simulations by dMORP, i.e., the enzyme levels did not change so considerably as the fluxes (Fig. 4). This could be explained by the control of metabolites, rather than gene expression, over glycolytic fluxes[41,42].

To compare with dMORP, we performed simulations by constraining exchange rates with measurements and minimizing the total proteome (Materials and Methods), and thus estimated the most efficient usage of the enzymes that maintain the experimentally observed metabolic states. This manner, which is widely adopted for enzyme-constrained simulations[34,43], performed worse than dMORP in terms of simulating the dynamics of the enzyme usage (Supplementary Fig. 12). In addition, this indicates suboptimal performance of enzymes during the transition, which could be associated with enzyme occupancy by substrates and thermodynamics[44].

In conclusion, the model simulations and experimental measurements demonstrated that the cellular proteome tended to maintain minimal adjustment upon rapid environmental changes, i.e., after glucose depletion cells utilized the proteome expressed on glucose phase to consume trehalose. In addition, the flux through the phosphoketolase pathway did not decrease so much as the glycolytic flux, which led to an increased fraction of carbon source toward phosphoketolase pathway and thus lowered lactate yield.

**Evolved strains performed homolactic fermentation by co-utilizing the mixed carbon sources**

To circumvent the hierarchical utilization, we carried out ALE (Fig. 5A) and obtained four evolved strains that can co-utilize glucose and trehalose (Supplementary Fig. 13). Whole-genome

sequencing identified the mutation in the gene *crr* encoding glucose-specific phosphotransferase enzyme IIA component in all evolved strains (Supplementary Table 2), in line with the findings of the microbes with diminished glucose repression[45-47].

We grew one of the evolved strains Ev3 on the mixture of glucose and trehalose in the 5 L bioreactor cultivation and monitored biomass and extracellular metabolite levels (Supplementary Fig. 14). We found that Ev3 utilized glucose and trehalose simultaneously until 14 h when trehalose was exhausted, and then glucose served as the sole carbon source. By calculating the lactate yield for these two phases, we found that Ev3 performed homolactic fermentation on both phases, which led to a higher total lactate yield than the wildtype strain (Supplementary Fig. 14).

In addition, the dynamics from mixed carbon sources to glucose utilization provided another scenario that could test MORP. To this end, we simulated the fermentation process of Ev3 within the dFBA framework, in which the first phase (before 14 h) was simulated by maximizing growth and the second (after 14 h) by MORP. We showed that MORP could also capture the physiological changes after trehalose depletion (Fig. 5B), and thus foresee more applications of MORP.

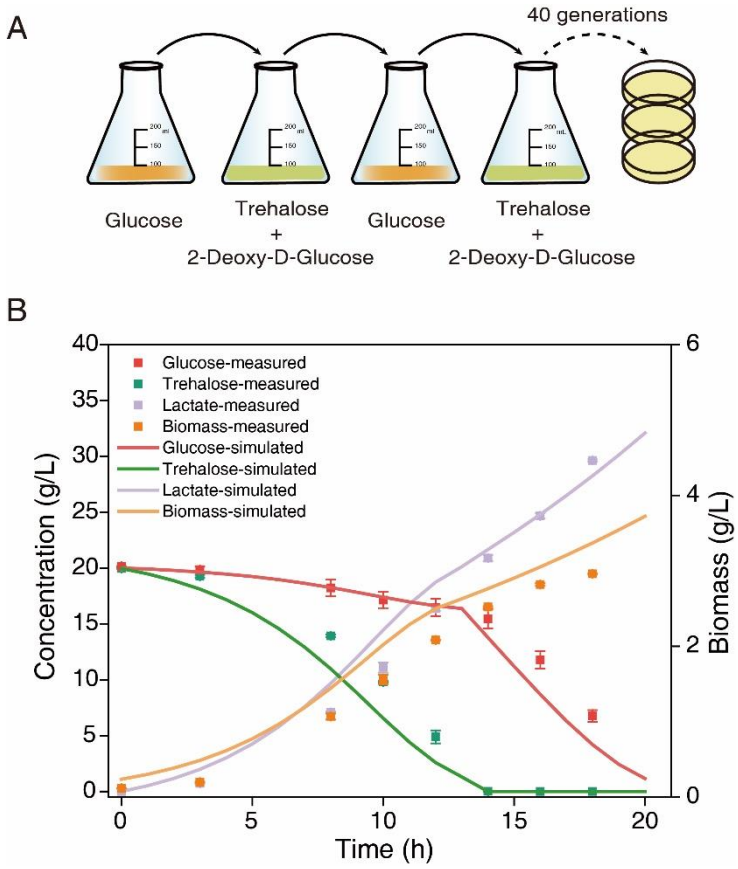


**Figure 5. Adaptive laboratory evolution and fermentation process of the evolved strain.** (A) Brief diagram of adaptive laboratory evolution experiment. The addition of 2-Deoxy-D-glucose to trehalose aimed at efficiently utilizing trehalose in the absence of glucose, with the intention of

eliminating the catabolite repression effect. After 40 generations, growth and lactate production were basically stable. The strains with notably improved lactate production were selected for subsequent shake flasks validation and 5 L bioreactor experiments. (B) Fermentation with mixed carbon sources in 5 L bioreactor by the evolved strain Ev3. Simulations were performed for the fermentation process, in which dFBA with maximization of growth was performed in the phase of simultaneous utilization of glucose and trehalose and dMORP was performed after trehalose depletion. Data are shown with mean ± s.d. of three biological replicates.

## Discussion

Here, we observed that *B. coagulans* utilized glucose and trehalose hierarchically and transitioned from homolactic to heterolactic fermentation during the hierarchical utilization (Fig. 1). We hypothesized that the dynamic minimization of proteome reallocation might result in this observation. To test it, we reconstructed the enzyme-constrained genome-scale metabolic model of *B. coagulans*, and developed MORP and its dynamic version dMORP. The model with dMORP accurately simulated the transition from homolactic to heterolactic fermentation of *B. coagulans* (Fig. 2), and the noticeable reduction in the glycolytic fluxes while subtle reduction in the gene expression levels of glycolytic enzymes, validated by the omics data (Fig. 4). Moreover, we evolved strains to circumvent the hierarchical utilization and prevent the metabolic transition. Therefore, we conclude that the dynamic minimization of proteome reallocation can explain the microbial choice of the metabolic strategies upon environmental changes, e.g., changes in the availability of carbon sources in the medium.

The biological basis of the minimization of proteome reallocation is the high cost and slow adjustment of protein synthesis and degradation[40,48,49] that the cells should consider when adapting to rapid perturbations. Additionally, the minimization of proteome reallocation is in line with the findings of proteome reserves[50,51], i.e., the proteome is not fully optimized for the environmental condition where the cells are living, as a suboptimal proteome could reduce the cost and time of reallocation upon the adaption to a new condition. By integrating the minimization of proteome reallocation into the constraint-based modeling framework, we developed MORP and dMORP that introduce the past proteome as an internal constraint, which provide additional objective functions for simulating cellular behaviors[52]. Particularly, dMORP would serve as a promising algorithm in the field of dynamic metabolic modeling to predict cellular kinetics[53,54] and history-dependent behaviors[48,55,56].

The approach of minimization of metabolic adjustment (MOMA) has been widely used to simulate cellular behaviors in response to genetic or environmental perturbations[57-59] by minimizing the sum of absolute changes in metabolic fluxes before and after perturbations[60]. Compared with minimizing the adjustment of metabolic fluxes, we argue that it is more biologically meaningful to minimize the adjustment of proteome, which now can be achieved by MORP using enzyme-constrained models. It should be noted that MORP can predict the mismatch between enzyme and flux levels, which appears to be an impossible mission for the MOMA approach implemented on conventional GEMs. In addition, it is less computationally expensive to perform the dynamic simulations on enzyme-constrained models than on fine-grained models, such as ME-models[61,62]

that explicitly formulate gene expression processes[26,63]. Therefore, we expect extensive applications of MORP and dMORP with the development of enzyme-constrained models[64].

In summary, we applied systems biology approaches to decipher the principles of the cellular response of *B. coagulans* upon the hierarchical utilization of mixed carbon sources, and identified the dynamic minimization of proteome reallocation to be the cellular objective that dominates the metabolic behavior in response to rapid environmental changes. In addition, we implemented the minimization of proteome reallocation as an effective objective function in the metabolic modeling framework, which would be useful for simulating and understanding cellular responses upon perturbations.

## Materials and Methods

### Microorganism, media and culture conditions

*B. coagulans* DSM 1 = ATCC 7050 was purchased from the American Type Culture Collection.

Seed medium was MRS medium[65], simplified chemically defined medium (CDM) used for fermentation in this study, i.e., MCDM3++, which was developed in our previous study[32]. 20 g/L glucose and 20 g/L trehalose were used as the mixed carbon source to better reproduce the phenomenon of hierarchical utilization.

Seed culture and shake flask fermentation were performed in 250 mL shake flasks with 100 mL working volume at 50 °C and 100 rpm, pH was buffered with $CaCO_3$. The cells in seed culture were collected and washed twice using 100 mM phosphate buffer at around 12 h. Collected cells were resuspended in ultrapure water with a determined volume and then transferred to the fermentation medium in shake flasks or 5 L bioreactors. Shake flask fermentation was used to investigate the metabolic properties of different combinations of mixed carbon sources.

Batch fermentation was performed in a 5 L bioreactor with 4 L working volume at 50 °C, 100 rpm and 7.2 L/h aeration, and pH was automatically controlled at 5.5 using 25% w/v $Ca(OH)_2$. The samples of different phases were collected for determination of biomass, metabolites, transcriptome and proteome. Fermentations were performed in triplicates for all conditions.

### Determination of biomass and metabolites

The optical density (OD) was detected using a spectrophotometer at 620 nm to characterize the biomass concentration.

Lactate, acetate, citate, pyruvate and acetoin in the fermentation broth were determined by high performance liquid chromatography (HPLC) (Shimadzu LC‐20AT)[13]. The Hi-Plex H (300 mm × 7.7 mm) column was used with 210 nm wavelength and 50 °C column temperature; the mobile phase was 0.01 mol/L sulfuric acid solution and the flow rate was set to 0.4 mL/min. The HPLC detection method for ethanol is as follows: the Aminex HPX-87H (300 mm × 7.8 mm) column was used with refractive index detector and 60 °C column temperature; the mobile phase was 0.01 mol/L sulfuric acid solution and the flow rate was set to 0.6 mL/min.

The carbon sources in the fermentation broth were determined by ion chromatography (Dionex ICS-3000) with Dionex Carbopac PA 20 column, the method was referred to the previous description[30] and modified. The pretreatment process of the samples was performed as follows: 1) The samples were diluted to achieve sugar concentrations within the detection range. 2) $Na_2C_2O_4$ was used to precipitate calcium ions in the culture medium. 3) Proteins were removed from the samples using ethanol. 4) The processed solution was evaporated to obtain the solid form of the sugar, which was then dissolved in water to obtain the sample for testing. The mobile phase was ultrapure water and 200 mmol/L NaOH, respectively. The elution procedure was ultrapure water and 200 mmol/L NaOH eluted at 9:1 ratio for 18 min, then adjusted the ratio to 2:8 to elute for 17 min, and finally adjusted to 9:1 to balance the column for 35 min, and the flow rate for the entire process was set to 0.4 mL/min.

**Reconstruction of genome-scale metabolic models**

The model iBcoa620 was reconstructed based on the model iBag597[14]: 1) A combined draft model from KEGG[66] and MetaCyc[67] pathway databases based on the genome sequences of *B. coagulans* DSM 1 = ATCC 7050 (GCF_000832905.1) was reconstructed by RAVEN 2.4.0[68]. 2) Another draft model was reconstructed by ModelSEED[69] database based on the genome annotation of RAST[70]. 3) Shared reactions in the draft models were integrated with iBag597. 4) The IDs of genes, metabolites, and reactions were unified into the form of the KEGG database. 5) Reactions with mass imbalance were corrected. 6) The memote score system was used to assess the model quality. 7) The model was validated by comparing the predicted and measure growth rates under different carbon sources.

The enzyme-constrained model eciBcoa620 was reconstructed using the GECKO toolbox 3.0. Note that $k_{cat}$ values were obtained from BRENDA[71] and GotEnzymes[72] databases and predicted using DLKcat tool[73]. Molecular weights of all enzymes were obtained from UniProt[74] database.

**Simulation methods**

MORP is implemented on the enzyme-constraint models, which can estimate both metabolic and enzyme usage fluxes. MORP estimates the metabolic and enzyme usage fluxes of the model upon a perturbation based on the minimization of proteome reallocation. Thus, the fluxes of the model from a reference condition should be used as the input of MORP, which can be obtained in advance by other algorithms, e.g., FBA, with the enzyme-constraint models. The core of MORP is to minimize the sum of absolute differences of enzyme usage fluxes between the reference and the perturbed conditions:

$$\min \quad \sum_{\mathrm{i}=1}^{\mathrm{m}} \left| v_{\mathrm{enzyme,i,perturb}} - v_{\mathrm{enzyme,i,ref}} \right|$$

$$\text{subject to} \quad \boldsymbol{S} \cdot \boldsymbol{v} = \boldsymbol{0}$$

$$lb_{\mathrm{j}} \leq v_{\mathrm{j}} \leq ub_{\mathrm{j}}$$

where $v_{enzyme,i,perturb}$ and $v_{enzyme,i,ref}$ represent fluxes of enzyme usage reaction i under perturbed and reference conditions, and m represents the total number of enzyme usage reactions in the model. As MORP estimates fluxes for the perturbed condition, $\boldsymbol{S}$ and $\boldsymbol{v}$ represent the stoichiometric matrix and flux vector of the model for the perturbed condition, and $v_j$, $lb_j$ and $ub_j$ are the flux, lower and upper bounds of the reaction j, respectively.

dFBA was used to simulate for the hierarchical utilization of glucose and trehalose, in which an objective function should be determined for different time intervals. As mentioned before three objective functions were used, i.e., maximization of growth, lactate production and NGAM. Generally, dFBA solves:

$$\max \quad v_{\mathrm{o,k}} \quad \mathrm{k} \in \mathrm{N}$$

$$\text{subject to} \quad \boldsymbol{S} \cdot \boldsymbol{v} = \boldsymbol{0}$$

$$v_{\mathrm{s,k}} = \frac{v_{\mathrm{s,max}}[S]_{\mathrm{k-1}}}{K_{\mathrm{m}} + [S]_{\mathrm{k-1}}}$$

$$lb_{\mathrm{j}} \leq v_{\mathrm{j}} \leq ub_{\mathrm{j}}$$

where k represents the $k_{th}$ time interval, N represents the number of time intervals of the phase of interest and thus is a positive integer, $v_{o,k}$ is the flux of the objective reaction in $P_{gluc}$, i.e., the biomass formation, or the flux of the objective reaction after glucose depletion, i.e., the biomass formation, lactate production, or NGAM production, $v_{s,k}$ is the flux of the uptake reaction of the sugar, i.e., glucose or trehalose, of the kth time interval, $[S]_{k-1}$ is the sugar concentration of the $(k-1)_{th}$ time interval, $v_{s,max}$ is the maximum sugar uptake rate, and $K_m$ is the sugar saturation constant.

dMORP was proposed to simulate the entire period after glucose depletion in the hierarchical utilization of glucose and trehalose. Here dMORP solves:

$$\min \quad \sum_{i=1}^{m} \left| v_{\mathrm{enzyme,i,r}} - v_{\mathrm{enzyme,i,r-1}} \right| \quad \mathrm{r} \in \mathrm{N}$$

$$\text{subject to} \quad \boldsymbol{S} \cdot \boldsymbol{v} = \boldsymbol{0}$$

$$v_{\mathrm{s,r}} = \frac{v_{\mathrm{s,max}}[S]_{\mathrm{r-1}}}{K_{\mathrm{m}} + [S]_{\mathrm{r-1}}}$$

$$lb_{\mathrm{j}} \leq v_{\mathrm{j}} \leq ub_{\mathrm{j}}$$

where r represents the $r_{th}$ time interval after glucose depletion, N represents the number of time intervals of the phase of interest and thus is a positive integer, $v_{enzyme,i,r}$ and $v_{enzyme,i,r-1}$ represent the flux of enzyme usage reaction i for the $r_{th}$ and $(r-1)_{th}$ time interval, respectively, $v_{s,r}$ is the flux of the trehalose uptake reaction of the $r_{th}$ time interval, and $[S]_{r-1}$ is the trehalose concentration of the $(r-1)_{th}$ time interval.

Minimization of the total proteome was performed to estimate the most efficient usage of the enzymes that maintain the experimentally observed metabolic states:

$$\min \quad v_{\text{total proteome}}$$

$$\text{subject to} \quad \boldsymbol{S} \cdot \boldsymbol{v} = \boldsymbol{0}$$

$$lb_{\text{i}} \leq v_{\text{i}} \leq ub_{\text{i}}$$

where $v_{\text{total proteome}}$ represents the flux of total proteome usage, $v_{\text{i}}$ represents the flux of exchange reaction of detected extracellular metabolite, $lb_{\text{i}}$ and $ub_{\text{i}}$ are lower and upper bounds based on measurements.

All the simulations were performed with the COBRA toolbox 3.0[75] on Matlab R2019a, and the solver was Gurobi 9.1 (https://www.gurobi.com/).

**Transcriptome analysis**

Cells in the fermentation broth were collected and washed three times with phosphate buffer saline for subsequent RNA extraction. Total RNA was isolated from cells using TRIzol Reagent following the instructions and genomic DNA was removed using DNase I (TaKara). Subsequently, RNA quality was determined using a Agilent2100 Bioanalyzer and quantified using ND-2000 (NanoDrop Technologies).

RNA library construction was performed using TruSeqTM RNA sample preparation Kit from Illumina (San Diego, CA). The rRNA was removed using Ribo-Zero Magnetic kit (epicenter), and double-stranded cDNA was reverse transcribed using random primers (Illumina) and SuperScript double-stranded cDNA synthesis kit (Invitrogen, CA). To synthesize the second strand of cDNA, it uses dUTP instead of dTTP, and then eliminates the second strand of cDNA containing dUTP, so that the library contained only the first strand of cDNA. After PCR amplification by Phusion DNA polymerase (NEB) and TBS380 (Picogreen) quantification, paired-end RNA-seq sequencing library was sequenced with the Illumina Novaseq (2 × 150bp read length).

The data generated from Illumina platform were used for bioinformatics analysis, and the reference genome and gene annotation files of *B. coagulans* DSM 1 = ATCC 7050 were downloaded from the National Center for Biotechnology Information. All of the analyses were performed using the free online platform of Majorbio Cloud Platform (www.majorbio.com).

**Proteome analysis**

Cells in the fermentation broth were collected and washed three times with phosphate buffer saline for subsequent protein extraction. Sample lysis and protein extraction were performed using SDT (4% SDS, 100 mM Tris-HCl, 1 mM DTT, pH 7.6) buffer, and the protein was quantified using the BCA Protein Assay Kit (Bio-Rad, USA). Protein digestion was performed with trypsin following the filter-aided sample preparation (FASP) procedure. The digested peptides from each sample were subsequently desalted (Empore™ SPE Cartridges C18 (standard density), bed I.D. 7 mm, volume 3 mL, Sigma) and concentrated. The protein for each sample were quantified by

SDS-PAGE. 100 μg peptide mixture for each sample was labeled using TMT reagent according to the instructions (Thermo Scientific). The labeled peptides were separated by High pH Reversed-Phase Peptide Fractionation Kit (Thermo Scientific) to obtain 10 different fractions, the collected fractions were desalted on C18 Cartridges and concentrated.

LC-MS/MS analysis was performed using a Thermo Scientific Q Exactive mass spectrometer equipped with the Easy nLC system (Proxeon Biosystems, Thermo Fisher Scientific). Peptides were trapped on a reverse phase trap column (Thermo Scientific Acclaim PepMap100, 100 μm × 2 cm, nanoViper C18) and separated on the C18-reversed phase analytical column (Thermo Scientific Easy Column, 10 cm long, 75 μm inner diameter, 3 μm resin). The separation was achieved using buffer A (0.1% formic acid) and buffer B (84% acetonitrile and 0.1% formic acid) at a constant flow rate of 300 nL/min controlled by IntelliFlow technology. The mass spectrometer was operated in positive ion mode. MS/MS analysis was performed using the data-dependent top10 method for high-energy collision dissociation (HCD) fragmentation by selecting the most abundant precursor ion (300-1800 m/z) in the measurement scan. The MS raw data was subjected to identification and quantitative analysis using MASCOT engine (Matrix Science, London, UK; version 2.2) and Proteome Discoverer 1.4 software. The proteome detection and analysis process were conducted in shanghai applied protein technology co.ltd.

**Differential expression analysis**

Significance analysis between two conditions or phases were performed using the two-sided *t*-test, and a cut-off adjusted *P* value ($P_{adjusted}$) of 0.01 was adopted for identifying differentially expressed transcripts and proteins based on transcriptomics and proteomics data.

**Determination of intracellular metabolites**

The absolute quantification of intracellular amino acids was performed using gas chromatography-mass spectrometry (Agilent, GC-7890A, MS-5975C). Before the extraction of intracellular metabolites, a quenching step was performed to terminate cell metabolism. 2 mL of fermentation broth were added to a 50 mL centrifuge tube containing 30 mL of 60% methanol pre-cooled to -27 °C. After quenching for 5 minutes, filter paper with attached cells was obtained by filtration. Simultaneously, 100 μL of U-$^{13}$C-labeled cell extracts was added to the filter paper as internal standards. The filter paper was then placed in a 75% ethanol solution pre-heated to 80 °C and boiled for 5 min. The filter paper was removed, and the remaining liquid was concentrated to 600 μL using rapid evaporation. A 100 μL portion was taken as the sample and subjected to freeze-drying before derivatization[14,76,77].

Amino acids derivatization method: 100 μL of pyridine was added to the freeze-dried sample, and the mixture was dissolved in a 65 °C for 1 hour. After the sample reached room temperature, 100 μL of derivatization reagent (N‐tert‐butyldimethylsilyl‐N-methyl-trifluoroacetamide with 1% tert‐butyldimethylchlorosilane) was added, and derivatization was carried out in a 65 °C oven for 1 hour. The sample was then centrifuged at 12000 rpm for 5 min, and the supernatant was subjected to GC-MS analysis.

The GC-MS detection conditions were as follows: the interface temperature of the GC-MS was set at 280 °C, the transfer line temperature was 250 °C, Ionization was done by electron impact with the temperature being 230 °C, the quadrupole temperature was 150 °C, and the injection volume was 1 μL. The chromatographic column used was HP-5MS with dimensions of 30 mm × 0.25 mm × 0.25 μm. For amino acids, the temperature program consisted of an initial column temperature of 100 °C for 1 minute, followed by an increase at a rate of 10 °C/min to reach 320 °C, which was then maintained for 10 minutes.

**Adaptive laboratory evolution**

The adaptive laboratory evolution strategy was performed in a 250 mL shake flask with complex medium, 100 rpm, 50 °C. Alternating cultures of glucose and trehalose were utilized, while the trehalose was supplemented with glucose structural analogue (2-deoxy-D-glucose), which can be absorbed but not be metabolized, so it can be used for screening mutant strains without catabolite repression effect [78,79]. The hope was to obtain strains that could utilize glucose and trehalose simultaneously. During the evolution process, the cells were transferred to new medium in the exponential phase and maintained the same concentration ($OD_{620}$ about 0.5) after inoculation. The initial total sugar concentration during evolution was kept constant at 130 g/L (glucose 130 g/L, 2-deoxy-D-glucose 40 g/L + trehalose 90 g/L), and the concentration of 2-deoxy-D-glucose was determined according to our previous study. Four evolved strains with the expected phenotypes were examined by MRS plate culture, and the strain with faster sugar consumption rate and higher lactate yield was selected for fermentation experiments in 5 L bioreactor.

**Whole-genome sequencing**

Cells from the exponential phase in seed shake flasks were collected for genome sequencing. Genomic DNA of *B. coagulans* DSM 1 = ATCC 7050 was extracted using Wizard Genomic DNA Purification Kit (Promega) according to the protocol. Purified genomic DNA was quantified by TBS-380 fluorometer (Turner BioSystems Inc., Sunnyvale, CA). Whole-genome sequencing of wildtype strain and four evolved strains was performed using the de novo sequencing method based on the Illumina NovaSeq6000 platform in this study. The final genome of five strains were annotated from KEGG, GO, COG and other databases using BLASTP, Diamond and HMMER. The same mutated genes of four evolved strains were considered to be genes that could cause phenotypic change.

**Data availability**

The genome sequences of four evolved strains have been deposited in NCBI database under the BioProject accession number of PRJNA1012373. The transcriptomics data have been deposited in NCBI database under the BioProject accession number of PRJNA1012495. The mass spectrometry proteomics datasets have been deposited in the ProteomeXchange with the dataset identifier PXD045169.

**Code availability**

The models and code are available at https://github.com/ChenYuGroup/MORP.

**Acknowledgments**

This study was financially supported by the National Key R&D Program of China (2023YFA0913900), the Shenzhen Medical Research Fund (A2303026) and the National Natural Science Foundation of China (21878084).

**Author contributions**

Y.C. and Y.W. conceived the study. Z.L., M.C. and J.H. performed the experiments. Z.L. and Y.C. constructed the models and performed the simulations. Z.L. and Y.C. analyzed the data. Y.C., Z.L. and Y.W. wrote the paper. All authors approved the final paper.

**Competing Interest:** The authors declare no competing interests.

**References**

1 Heiden, M. G. V., Cantley, L. C. & Thompson, C. B. Understanding the Warburg Effect: The Metabolic Requirements of Cell Proliferation. *Science* **324**, 1029-1033, doi:10.1126/science.1160809 (2009).

2 Shen, Y. *et al.* Mitochondrial ATP generation is more proteome efficient than glycolysis. *Nat. Chem. Biol.*, doi:10.1038/s41589-024-01571-y (2024).

3 Pfeiffer, T., Schuster, S. & Bonhoeffer, S. Cooperation and competition in the evolution of ATP-producing pathways. *Science* **292**, 504-507, doi:10.1126/science.1058079 (2001).

4 Molenaar, D., van Berlo, R., de Ridder, D. & Teusink, B. Shifts in growth strategies reflect tradeoffs in cellular economics. *Mol. Syst. Biol.* **5**, 323, doi:10.1038/msb.2009.82 (2009).

5 Flamholz, A., Noor, E., Bar-Even, A., Liebermeister, W. & Milo, R. Glycolytic strategy as a tradeoff between energy yield and protein cost. *Proc. Natl. Acad. Sci. U. S. A.* **110**, 10039-10044, doi:10.1073/pnas.1215283110 (2013).

6 Szenk, M., Dill, K. A. & de Graff, A. M. R. Why Do Fast-Growing Bacteria Enter Overflow Metabolism? Testing the Membrane Real Estate Hypothesis. *Cell Syst.* **5**, 95-104, doi:10.1016/j.cels.2017.06.005 (2017).

7 Du, B., Zielinski, D. C., Monk, J. M. & Palsson, B. O. Thermodynamic favorability and pathway yield as evolutionary tradeoffs in biosynthetic pathway choice. *Proc. Natl. Acad. Sci. U. S. A.* **115**, 11339-11344, doi:10.1073/pnas.1805367115 (2018).

8 Mori, M., Marinari, E. & De Martino, A. A yield-cost tradeoff governs *Escherichia coli*'s decision between fermentation and respiration in carbon-limited growth. *NPJ Syst Biol Appl* **5**, 16, doi:10.1038/s41540-019-0093-4 (2019).

9 Basan, M. *et al.* Overflow metabolism in *Escherichia coli* results from efficient proteome allocation. *Nature* **528**, 99-104, doi:10.1038/nature15765 (2015).

10 Chen, Y. & Nielsen, J. Energy metabolism controls phenotypes by protein efficiency and allocation. *Proc. Natl. Acad. Sci. U. S. A.* **116**, 17592-17597, doi:10.1073/pnas.1906569116 (2019).

11 Schuetz, R., Zamboni, N., Zampieri, M., Heinemann, M. & Sauer, U. Multidimensional Optimality of Microbial Metabolism. *Science* **336**, 601-604, doi:10.1126/science.1216882

(2012).

12 Mori, M., Schink, S., Erickson, D. W., Gerland, U. & Hwa, T. Quantifying the benefit of a proteome reserve in fluctuating environments. *Nat. Commun.* **8**, doi:10.1038/s41467-017-01242-8 (2017).

13 Lv, X. *et al.* Effect of pH, glucoamylase, pullulanase and invertase addition on the degradation of residual sugar in L-lactic acid fermentation by *Bacillus coagulans* HL-5 with corn flour hydrolysate. *J. Taiwan Inst. Chem. Eng.* **61**, 124-131, doi:10.1016/j.jtice.2016.01.007 (2016).

14 Chen, Y. *et al.* Genome-scale modeling for *Bacillus coagulans* to understand the metabolic characteristics. *Biotechnol. Bioeng.* **117**, 3545-3558, doi:10.1002/bit.27488 (2020).

15 Gaenzle, M. G. Lactic metabolism revisited: metabolism of lactic acid bacteria in food fermentations and food spoilage. *Curr. Opin. Food Sci.* **2**, 106-117, doi:10.1016/j.cofs.2015.03.001 (2015).

16 Wang, Y. *et al.* Metabolism Characteristics of Lactic Acid Bacteria and the Expanding Applications in Food Industry. *Front. Bioeng. Biotechnol.* **9**, 612285, doi:10.3389/fbioe.2021.612285 (2021).

17 Wang, Q., Ingram, L. O. & Shanmugam, K. T. Evolution of D-lactate dehydrogenase activity from glycerol dehydrogenase and its utility for D-lactate production from lignocellulose. *Proc. Natl. Acad. Sci. U. S. A.* **108**, 18920-18925, doi:10.1073/pnas.1111085108 (2011).

18 Wang, L. *et al.* Jerusalem artichoke powder: A useful material in producing high-optical-purity L-lactate using an efficient sugar-utilizing thermophilic *Bacillus coagulans* strain. *Bioresour. Technol.* **130**, 174-180, doi:10.1016/j.biortech.2012.11.144 (2013).

19 Abdel-Rahman, M. A., Tashiro, Y. & Sonomoto, K. Recent advances in lactic acid production by microbial fermentation processes. *Biotechnol. Adv.* **31**, 877-902, doi:10.1016/j.biotechadv.2013.04.002 (2013).

20 Lu, Z., He, F., Shi, Y., Lu, M. & Yu, L. Fermentative production of L(+)-lactic acid using hydrolyzed acorn starch, persimmon juice and wheat bran hydrolysate as nutrients. *Bioresour. Technol.* **101**, 3642-3648, doi:10.1016/j.biortech.2009.12.119 (2010).

21 Hermsen, R., Okano, H., You, C., Werner, N. & Hwa, T. A growth-rate composition formula for the growth of *E. coli* on co-utilized carbon substrates. *Mol. Syst. Biol.* **11**, 801, doi:10.15252/msb.20145537 (2015).

22 Perrin, E. *et al.* Diauxie and co-utilization of carbon sources can coexist during bacterial growth in nutritionally complex environments. *Nat. Commun.* **11**, 3135, doi:10.1038/s41467-020-16872-8 (2020).

23 Okano, H., Hermsen, R. & Hwa, T. Hierarchical and simultaneous utilization of carbon substrates: mechanistic insights, physiological roles, and ecological consequences. *Curr. Opin. Microbiol.* **63**, 172-178, doi:10.1016/j.mib.2021.07.008 (2021).

24 Solopova, A. *et al.* Bet-hedging during bacterial diauxic shift. *Proc. Natl. Acad. Sci. U. S. A.* **111**, 7427-7432, doi:10.1073/pnas.1320063111 (2014).

25 Okano, H., Hermsen, R., Kochanowski, K. & Hwa, T. Regulation underlying hierarchical and simultaneous utilization of carbon substrates by flux sensors in Escherichia coli. *Nat.*

*Microbiol* **5**, 206-215, doi:10.1038/s41564-019-0610-7 (2020).

26 Salvy, P. & Hatzimanikatis, V. Emergence of diauxie as an optimal growth strategy under resource allocation constraints in cellular metabolism. *Proc. Natl. Acad. Sci. U. S. A.* **118**, e2013836118, doi:10.1073/pnas.2013836118 (2021).

27 Sievert, C. *et al.* Experimental evolution reveals an effective avenue to release catabolite repression via mutations in XylR. *Proc. Natl. Acad. Sci. U. S. A.* **114**, 7349-7354, doi:10.1073/pnas.1700345114 (2017).

28 Gawand, P., Hyland, P., Ekins, A., Martin, V. J. J. & Mahadevan, R. Novel approach to engineer strains for simultaneous sugar utilization. *Metab. Eng.* **20**, 63-72, doi:10.1016/j.ymben.2013.08.003 (2013).

29 Ma, K. *et al.* Highly efficient production of optically pure L-lactic acid from corn stover hydrolysate by thermophilic *Bacillus coagulans*. *Bioresour. Technol.* **219**, 114-122, doi:10.1016/j.biortech.2016.07.100 (2016).

30 Lv, X., Guo, Y., Zhuang, Y. & Wang, Y. Optimization and validation of an extraction method and HPAEC-PAD for determination of residual sugar composition in L-lactic acid industrial fermentation broth with a high salt content. *Anal. Methods* **7**, 9076-9083, doi:10.1039/c5ay01703c (2015).

31 Wee, Y. J., Yun, J. S., Park, D. H. & Ryu, H. W. Isolation and characterization of a novel lactic acid bacterium for the production of lactic acid. *Biotechnol. Bioprocess Eng.* **9**, 303-308, doi:10.1007/bf02942348 (2004).

32 Chen, Y., Dong, F. & Wang, Y. Systematic development and optimization of chemically defined medium supporting high cell density growth of *Bacillus coagulans*. *Appl. Microbiol. Biotechnol.* **100**, 8121-8134, doi:10.1007/s00253-016-7644-z (2016).

33 Lieven, C. *et al.* MEMOTE for standardized genome-scale metabolic model testing. *Nat. Biotechnol.* **38**, 272-276, doi:10.1038/s41587-020-0446-y (2020).

34 Chen, Y. *et al.* Reconstruction, simulation and analysis of enzyme-constrained metabolic models using GECKO Toolbox 3.0. *Nat. Protoc.* **19**, 629-667, doi:10.1038/s41596-023-00931-7 (2024).

35 Alter, T. B., Blank, L. M. & Ebert, B. E. Proteome Regulation Patterns Determine *Escherichia coli* Wild-Type and Mutant Phenotypes. *mSystems* **6**, doi:10.1128/mSystems.00625-20 (2021).

36 Mao, Z. *et al.* ECMpy 2.0: A Python package for automated construction and analysis of enzyme-constrained models. *Synthetic and systems biotechnology* **9**, 494-502, doi:10.1016/j.synbio.2024.04.005 (2024).

37 Ye, C. *et al.* Improving lysine production through construction of an *Escherichia coli* enzyme-constrained model. *Biotechnol. Bioeng.* **117**, 3533-3544, doi:10.1002/bit.27485 (2020).

38 Orth, J. D., Thiele, I. & Palsson, B. O. What is flux balance analysis? *Nat. Biotechnol.* **28**, 245-248, doi:10.1038/nbt.1614 (2010).

39 Henriques, D. *et al.* A multiphase multiobjective dynamic genome-scale model shows different redox balancing among yeast species of the Saccharomyces genus in fermentation.

*mSystems* **6**, 10-1128 (2021).

40 Kafri, M., Metzl-Raz, E., Jona, G. & Barkai, N. The Cost of Protein Production. *Cell Rep* **14**, 22-31, doi:10.1016/j.celrep.2015.12.015 (2016).

41 Davidi, D. *et al.* Global characterization of in vivo enzyme catalytic rates and their correspondence to in vitro kcat measurements. *Proc. Natl. Acad. Sci. U. S. A.* **113**, 3401-3406, doi:10.1073/pnas.1514240113 (2016).

42 Daran-Lapujade, P. *et al.* The fluxes through glycolytic enzymes in *Saccharomyces cerevisiae* are predominantly regulated at posttranscriptional levels. *Proc. Natl. Acad. Sci. U. S. A.* **104**, 15753-15758, doi:10.1073/pnas.0707476104 (2007).

43 Domenzain, I. *et al.* Reconstruction of a catalogue of genome-scale metabolic models with enzymatic constraints using GECKO 2.0. *Nat. Commun.* **13**, doi:10.1038/s41467-022-31421-1 (2022).

44 Park, J. O. *et al.* Near-equilibrium glycolysis supports metabolic homeostasis and energy yield. *Nat. Chem. Biol.* **15**, 1001-1008, doi:10.1038/s41589-019-0364-9 (2019).

45 Oh, B.-R. *et al.* The production of 1,3-propanediol from mixtures of glycerol and glucose by a Klebsiella pneumoniae mutant deficient in carbon catabolite repression. *Bioresour. Technol.* **130**, 719-724, doi:10.1016/j.biortech.2012.12.076 (2013).

46 Zhao, M., Shi, D., Lu, X., Zong, H. & Zhuge, B. Co-production of 1,2,4-butantriol and ethanol from lignocellulose hydrolysates. *Bioresour. Technol.* **282**, 433-438, doi:10.1016/j.biortech.2019.03.057 (2019).

47 Liang, Q. *et al.* Comparison of individual component deletions in a glucose-specific phosphotransferase system revealed their different applications. *Sci Rep* **5**, 13200, doi:10.1038/srep13200 (2015).

48 Rothman, D. L., Moore, P. B. & Shulman, R. G. The impact of metabolism on the adaptation of organisms to environmental change. *Front. Cell. Dev. Biol.* **11**, 1197226, doi:10.3389/fcell.2023.1197226 (2023).

49 Scott, M. & Hwa, T. Shaping bacterial gene expression by physiological and proteome allocation constraints. *Nat. Rev. Microbiol.* **21**, 327-342, doi:10.1038/s41579-022-00818-6 (2023).

50 Wu, C. *et al.* Enzyme expression kinetics by *Escherichia coli* during transition from rich to minimal media depends on proteome reserves. *Nat. Microbiol* **8**, 347-359, doi:10.1038/s41564-022-01310-w (2023).

51 Yu, R. *et al.* Nitrogen limitation reveals large reserves in metabolic and translational capacities of yeast. *Nat. Commun.* **11**, 1881, doi:10.1038/s41467-020-15749-0 (2020).

52 Bernstein, D. B., Sulheim, S., Almaas, E. & Segre, D. Addressing uncertainty in genome-scale metabolic model reconstruction and analysis. *Genome Biol.* **22**, 1-22, doi:10.1186/s13059-021-02289-z (2021).

53 Erickson, D. W. *et al.* A global resource allocation strategy governs growth transition kinetics of *Escherichia coli*. *Nature* **551**, 119-123, doi:10.1038/nature24299 (2017).

54 Basan, M. *et al.* A universal trade-off between growth and lag in fluctuating environments. *Nature* **584**, 470-474, doi:10.1038/s41586-020-2505-4 (2020).

55 Cerulus, B. *et al.* Transition between fermentation and respiration determines history-dependent behavior in fluctuating carbon sources. *Elife* **7**, doi:10.7554/eLife.39234 (2018).

56 Vermeersch, L. *et al.* Do microbes have a memory? History-dependent behavior in the adaptation to variable environments. *Front. Microbiol.* **13**, 1004488, doi:10.3389/fmicb.2022.1004488 (2022).

57 Yu, J. S. L. *et al.* Microbial communities form rich extracellular metabolomes that foster metabolic interactions and promote drug tolerance. *Nat. Microbiol* **7**, 542-555, doi:10.1038/s41564-022-01072-5 (2022).

58 Ho, W.-C. & Zhang, J. Evolutionary adaptations to new environments generally reverse plastic phenotypic changes. *Nat. Commun.* **9**, 350, doi:10.1038/s41467-017-02724-5 (2018).

59 Vaud, S. *et al.* Engineering improved ethylene production: Leveraging systems biology and adaptive laboratory evolution. *Metab. Eng.* **67**, 308-320, doi:10.1016/j.ymben.2021.07.001 (2021).

60 Segrè, D., Vitkup, D. & Church, G. M. Analysis of optimality in natural and perturbed metabolic networks. *Proc. Natl. Acad. Sci. U. S. A.* **99**, 15112-15117, doi:10.1073/pnas.232349399 (2002).

61 Lloyd, C. J. *et al.* COBRAme: A computational framework for genome-scale models of metabolism and gene expression. *PLoS Comput. Biol.* **14**, e1006302, doi:10.1371/journal.pcbi.1006302 (2018).

62 Reimers, A.-M., Knoop, H., Bockmayr, A. & Steuer, R. Cellular trade-offs and optimal resource allocation during cyanobacterial diurnal growth. *Proc. Natl. Acad. Sci. U. S. A.* **114**, E6457-E6465, doi:10.1073/pnas.1617508114 (2017).

63 Yang, L., Ebrahim, A., Lloyd, C. J., Saunders, M. A. & Palsson, B. O. DynamicME: dynamic simulation and refinement of integrated models of metabolism and protein expression. *BMC Syst. Biol.* **13**, 1-15, doi:10.1186/s12918-018-0675-6 (2019).

64 Chen, Y. & Nielsen, J. Mathematical modeling of proteome constraints within metabolism. *Curr. Opin. Syst. Biol.* **25**, 50-56, doi:10.1016/j.coisb.2021.03.003 (2021).

65 David, A. N., Sewsynker-Sukai, Y. & Kana, E. B. G. Co-valorization of corn cobs and dairy wastewater for simultaneous saccharification and lactic acid production: Process optimization and kinetic assessment. *Bioresour. Technol.* **348**, doi:10.1016/j.biortech.2022.126815 (2022).

66 Kanehisa, M. & Goto, S. KEGG: Kyoto Encyclopedia of Genes and Genomes. *Nucleic Acids Res.* **28**, 27-30, doi:10.1093/nar/28.1.27 (2000).

67 Karp, P. D., Riley, M., Paley, S. M. & Pellegrini-Toole, A. The MetaCyc database. *Nucleic Acids Res.* **30**, 59-61, doi:10.1093/nar/30.1.59 (2002).

68 Wang, H. *et al.* RAVEN 2.0: A versatile toolbox for metabolic network reconstruction and a case study on Streptomyces coelicolor. *PLoS Comput. Biol.* **14**, e1006541, doi:10.1371/journal.pcbi.1006541 (2018).

69 Henry, C. S. *et al.* High-throughput generation, optimization and analysis of genome-scale metabolic models. *Nat. Biotechnol.* **28**, 977-U922, doi:10.1038/nbt.1672 (2010).

70 Aziz, R. K. *et al.* The RAST server: Rapid annotations using subsystems technology. *BMC Genomics* **9**, doi:10.1186/1471-2164-9-75 (2008).

71 Jeske, L., Placzek, S., Schomburg, I., Chang, A. & Schomburg, D. BRENDA in 2019: a European ELIXIR core data resource. *Nucleic Acids Res.* **47**, D542-D549, doi:10.1093/nar/gky1048 (2019).

72 Li, F., Chen, Y., Anton, M. & Nielsen, J. GotEnzymes: an extensive database of enzyme parameter predictions. *Nucleic Acids Res.* **51**, D583-D586, doi:10.1093/nar/gkac831 (2023).

73 Li, F. *et al.* Deep learning-based kcat prediction enables improved enzyme-constrained model reconstruction. *Nat. Catal.* **5**, 662-672, doi:10.1038/s41929-022-00798-z (2022).

74 Apweiler, R. *et al.* UniProt: the Universal Protein knowledgebase. *Nucleic Acids Res.* **32**, D115-D119, doi:10.1093/nar/gkh131 (2004).

75 Heirendt, L. *et al.* Creation and analysis of biochemical constraint-based models using the COBRA Toolbox v.3.0. *Nat. Protoc.* **14**, 639-702, doi:10.1038/s41596-018-0098-2 (2019).

76 Wang, G., Chu, J., Zhuang, Y., van Gulik, W. & Noorman, H. A dynamic model-based preparation of uniformly-13C-labeled internal standards facilitates quantitative metabolomics analysis of Penicillium chrysogenum. *J. Biotechnol.* **299**, 21-31, doi:10.1016/j.jbiotec.2019.04.021 (2019).

77 Liu, X. *et al.* Dynamic changes of metabolomics and expression of candicidin biosynthesis gene cluster caused by the presence of a pleiotropic regulator AdpA in *Streptomyces* ZYJ-6. *Bioprocess. Biosyst. Eng.* **42**, 1353-1365, doi:10.1007/s00449-019-02135-4 (2019).

78 Liang, J., van Kranenburg, R., Bolhuis, A. & Leak, D. J. Removing carbon catabolite repression in *Parageobacillus thermoglucosidasius* DSM 2542. *Front. Microbiol.* **13**, 985465, doi:10.3389/fmicb.2022.985465 (2022).

79 Veyrat, A., Monedero, V. & Perez-Martinez, G. Glucose transport by the phosphoenolpyruvate: mannose phosphotransferase system in *Lactobacillus casei* ATCC 393 and its role in carbon catabolite repression. *Microbiology* **140**, 1141-1149 (1994).